JAAS FULL PAPER
www.rsc.org/jaas

Hydrogen addition to an argon glow discharge: a numerical simulation†

Annemie Bogaerts

University of Antwerp, Department of Chemistry, Universiteitsplein 1, B-2610 Wilrijk-Antwerp, Belgium. E-mail: annemie.bogaerts@ua.ac.be

Received 3rd January 2002, Accepted 15th February 2002
First published as an Advance Article on the web 25th March 2002

The effect of hydrogen added to an argon glow discharge is investigated by use of a set of numerical models for the various species present in the plasma, *i.e.*, argon gas atoms, electrons, fast argon atoms, argon metastable atoms, Ar^+, ArH^+, H^+, H_2^+ and H_3^+ ions, H atoms and H_2 molecules, sputtered Cu atoms and the corresponding Cu^+ ions. These species are described by a combination of Monte Carlo and fluid models. The effect of hydrogen on various calculation results is investigated, such as the electrical characteristics, the density of the species and flux energy distribution functions, the relative contribution to production and loss processes for the various species, the sputtering rate and the ionization of copper. The hydrogen addition is varied from 0.1 to 10%, and the results are also compared to a pure argon discharge. The calculated electrical current and the density and flux of the electrons, Ar^+ ions, argon metastable atoms, sputtered Cu atoms and Cu^+ ions decrease considerably as a result of hydrogen addition. The densities of the hydrogen-related ions, *i.e.*, ArH^+, H^+, H_2^+ and H_3^+, appear to achieve a maximum at a certain hydrogen concentration, whereas the densities of the H atoms and H_2 molecules continue to increase with the addition of hydrogen. The calculated energy of the electrons, the various ions and the fast Ar^0 atoms remains more or less unaffected by the hydrogen concentration. The relative contribution to the cathode sputtering by hydrogen-related ions, especially by ArH^+, rises with hydrogen addition, but the overall sputtering flux is predicted to decrease. Finally, the ionization of the sputtered Cu atoms appears to decrease with hydrogen addition, mainly because of a drop in Penning ionization. The relative contribution of electron impact ionization seems to become relatively more important. This might explain observations in the literature in which a better correlation was reached in an argon–hydrogen discharge compared to a pure argon discharge, between measured relative sensitivity factors and values predicted by simple empirical equilibrium models.

1 Introduction

Recently, there has been increasing interest in the effect of small amounts of hydrogen on the analytical results of argon glow discharges.[1–7] It appears that the relative sensitivity factors (RSF) of different elements in glow discharge mass spectrometry (GDMS) are influenced by the addition of hydrogen.[1,2] More specifically, a better correlation can be obtained between measured RSF and values predicted with simple empirical equilibrium models,[1,2] which opens up possibilities for quantitative analysis with GDMS even when suitable standard reference materials are not available. Moreover, in glow discharge optical emission spectrometry (GD-OES) it has been demonstrated that some optical emission line intensities increase while others decrease when hydrogen is added.[3–6] This has some very important implications for the analysis of "real samples". Indeed, many applications exist where hydrogen is a major component of the sample itself, such as organic residues after rolling and degreasing, corrosion products and polymer coatings.[3] Additionally, some traces of hydrogen are always detected in a glow discharge, arising from residual moisture in the source and on the sample surface, gaseous hydrocarbons coming from the pre-vacuum oil-pumps, leakage of water vapor through porous samples, *etc.*[4] Because of the effects of hydrogen on the optical emission line intensities,[3–6] a good understanding of the role of hydrogen in a glow discharge plasma is important in order to include corrections of the hydrogen effect in quantification algorithms, especially for the analysis of thin films and other surface layers containing hydrogen.

Other investigations in analytical glow discharges have included the effect of hydrogen on the ion intensities in a fast flowing glow discharge, with gas mixing close to the ion exit in order not to disturb the discharge.[7] Finally, hydrogen Balmer lines have been investigated in argon–hydrogen mixtures in a Grimm-type glow discharge[8–10] to obtain information on reactions in the plasma,[8] on the electron density[9] and on the electric field distribution.[10]

Argon–hydrogen mixtures have also been studied in other kinds of discharges.[11–32] The effect of hydrogen was to cause a drop in ionization in the discharge, and in the argon ion and electron concentration.[11–13] Moreover, it has been recognized that the addition of hydrogen affects the sputter rates in glow discharges.[14,15] A number of papers have also reported the measurement of ion energy distributions in argon–hydrogen discharges.[16–18] Finally, a vast number of chemical reactions between argon and hydrogen species has been studied for conditions typically used in discharge plasmas,[19–32] providing useful information, such as cross sections and rate coefficients, for numerical investigations of argon–hydrogen discharges.

In a recent paper, we gave an overview of all possible reactions that might take place in an argon–hydrogen glow discharge in order to make qualitative predictions of the effect of hydrogen on the discharge behavior and on the analytical characteristics.[33] Based on these reactions, we have recently developed a comprehensive modeling network describing the behavior in an argon glow discharge with 1% hydrogen

†Presented at the 2002 Winter Conference on Plasma Spectrochemistry, Scottsdale, AZ, USA, January 6–12, 2002.

 DOI: 10.1039/b200025c

added.[34] Ten different species were taken into account in that model, including electrons, Ar^+, ArH^+, H^+, H_2^+ and H_3^+ ions, fast argon atoms, H atoms and H_2 molecules, as well as argon metastable (Ar_m*) atoms. These species were found to interact with each other by using a large number of processes. More than 60 reactions were taken into account, including ionization, excitation, charge transfer, proton transfer, H-atom transfer, collision-induced dissociation and elastic collisions between different species.

In the present paper, the model developed in ref. 34 is extended by adding two more species, *i.e.*, the sputtered Cu atoms and the corresponding Cu^+ ions. The different species are described by a number of fluid models and Monte Carlo simulations, which form a large modeling network. The models are briefly described and the results, *i.e.*, the effect of different H_2 concentrations on the discharge behavior, are presented.

2 Description of the modeling network

Table 1 gives a list of the species taken into account in the modeling network and the models used to describe their behavior. No model is used for the argon gas atoms, which are assumed to be uniformly distributed in the plasma with thermal velocities. Their density is calculated from the input gas pressure and temperature, by the ideal gas law ($n = N/V = p/kT$) multiplied further by the percentage of argon (*i.e.*, 1 − percentage hydrogen).

The electrons are described in the entire discharge with a Monte Carlo model. The reactions taken into account in this model are given in Table 2. Because the thresholds of some of these reactions are rather low (*e.g.*, 0.5 eV for vibrational excitation of H_2), all electrons including the slow ones are described with this Monte Carlo model. Also, all the electrons are described using the fluid approach, together with the various ions (see below). This fluid model consists of continuity equations and transport equations (based on diffusion and migration in the electric field) for all the species (electrons and various ions). The continuity equations contain various production and loss terms, for which the rates are calculated in the Monte Carlo model and/or in the fluid code itself (based on the reaction rate coefficients multiplied by the densities of the colliding particles). A detailed overview of the production and loss processes taken into account in this model can be found in ref. 34. Finally, these continuity and transport equations are also used with Poisson's equation for a self-consistent calculation of the electric field. Summarized, the electrons are described by two models: the Monte Carlo model serves to calculate, in the most accurate way, the electron reactions and the electron energy distribution function, whereas the fluid approach allows a self-consistent calculation of the electric field (by coupling the Poisson equation to the electron continuity equation).

Table 1 Species taken into account in the modeling network and the models used to describe their behaviour

Plasma species	Model
Argon gas atoms	No model
Electrons	Monte Carlo model
	Fluid model
Ar^+ ions	Fluid model
	Monte Carlo model in the CDS
ArH^+ ions	Fluid model
	Monte Carlo model in the CDS
H^+ ions	Fluid model
	Monte Carlo model in the CDS
H_2^+ ions	Fluid model
	Monte Carlo model in the CDS
H_3^+ ions	Fluid model
	Monte Carlo model in the CDS
Fast Ar^0 atoms	Monte Carlo model in the CDS
H atoms	Fluid model
H_2 molecules	Fluid model
Ar metastable atoms (Ar_m*)	Fluid model
Cu^0 sputtering	Empirical formula
Cu^0 atoms: thermalization	Monte Carlo model
Thermal Cu^0 atoms	Fluid model
Cu^+ ions	Fluid model
	Monte Carlo model in the CDS

The Ar^+, ArH^+, H^+, H_2^+ and H_3^+ ions are also described by this fluid code. In addition, they are also described in the cathode dark space (CDS), *i.e.*, the region near the cathode characterized by a strong electric field, by a Monte Carlo method. Indeed, in this region, the ions are not in equilibrium with the strong electric field, and they are more accurately represented with a Monte Carlo model, which gives a more correct description of their collision processes and which allows the computation of the ion energy distribution functions needed to calculate the sputtering rate. Similarly, a Monte Carlo model is also applied in the CDS for the fast argon atoms, which are created from collisions of the various ionic species in this region. The most important output of this fast argon atom Monte Carlo model is the flux energy distribution of the fast argon atoms needed to calculate the sputtering rate. The collisions taken into account in the Ar^+, ArH^+, H^+, H_2^+, H_3^+ and fast Ar^0 Monte Carlo models are also summarized in Table 2. More detailed information about these Monte Carlo models and the included reactions is given in ref. 34.

The behavior of the H atoms and H_2 molecules is calculated in a fluid model in the entire discharge, which consists again of two continuity equations with different production and loss processes (see ref. 34 for an overview) and two transport equations (based on diffusion). A similar fluid model is also constructed for the argon metastable atoms in the entire discharge. The production and loss mechanisms were presented previously in ref. 35, but two additional loss processes specific to the argon/hydrogen discharge are taken into account, *i.e.*, quenching by H_2 molecules and excitation of H atoms.[34]

All these models, as well as their interactions, were extensively described in ref. 34, and the interested reader is therefore referred to this paper. In addition, three models describing the behavior of the sputtered species are now used with the above-mentioned models and will be briefly outlined here. The sputtering rate for the copper cathode is calculated based on an empirical formula for the sputtering yield, multiplied by the flux energy distribution of the various ions and the fast argon atoms bombarding the cathode. The copper atoms sputtered from the cathode have typical energies of the order of 5–10 eV, which are almost immediately lost by collisions with the argon gas atoms, until the copper atoms are thermalized. This thermalization process is described with a Monte Carlo model.

The further behavior of the thermalized copper atoms, *i.e.*, their transport by diffusion, the ionization of copper atoms and the behavior of the Cu^+ ions, is described with a fluid model consisting of two coupled continuity equations (*i.e.*, for the copper atoms and the Cu^+ ions) and two transport equations (based on diffusion of the copper atoms and on diffusion + migration of the Cu^+ ions). The rate of production of copper atoms is given by the product of the sputtering rate and the thermalization profile, whereas the loss of copper atoms is dictated by electron impact ionization, Penning ionization by argon metastable atoms and asymmetric charge transfer with Ar^+ ions. Hence, the copper atom loss rate is equal to the Cu^+ ion production rate.

Finally, a Monte Carlo method was also developed for the Cu^+ ions in the CDS, because they are not in equilibrium with the strong electric field in this region, and because this Monte Carlo method allows the Cu^+ ion flux energy distribution, needed for the sputtering rate, to be calculated. More details about these models for the Cu atoms and Cu^+ ions can be found in refs. 36–38.

Table 2 Reactions taken into account in the Monte Carlo models

Electron Monte Carlo model—	
Elastic scattering	$e^- + Ar \rightarrow e^- + Ar$
Ionization	$e^- + Ar \rightarrow e^- + Ar^+ + e^-$
Total excitation (including up to the Ar metastable levels)	$e^- + Ar \rightarrow e^- + Ar^*$ (incl. Ar_m^*)
Ionization from the Ar metastable levels	$e^- + Ar_m^* \rightarrow e^- + Ar^+ + e^-$
Total excitation from the Ar metastable levels	$e^- + Ar_m^* \rightarrow e^- + Ar^*$
Elastic scattering	$e^- + H_2 \rightarrow e^- + H_2$
Total vibrational excitation	$e^- + H_2 \rightarrow e^- + H_2^*$ (v)
Total electron excitation to singlet states	$e^- + H_2 \rightarrow e^- + H_2^*$ (s)
Total electron excitation to triplet states, followed by dissociation	$e^- + H_2 \rightarrow e^- + H_2^*$ (t) $\rightarrow e^- + H + H$
Ionization	$e^- + H_2 \rightarrow e^- + H_2^+ + e^-$
Dissociative ionization	$e^- + H_2 \rightarrow e^- + H^+ + H + e^-$
Total excitation	$e^- + H \rightarrow e^- + H^*$
Ionization	$e^- + H \rightarrow e^- + H^+ + e^-$
Ar^+ Monte Carlo model—	
Elastic (isotropic) scattering	$Ar^+ + Ar \rightarrow Ar^+ +$ fast Ar
Elastic scattering in backward direction (or so-called "symmetric charge transfer")	$Ar^+ + Ar \rightarrow$ fast Ar + slow Ar^+
Ionization	$Ar^+ + Ar \rightarrow Ar^+ + Ar^+ + e^-$
Excitation to the metastable levels	$Ar^+ + Ar \rightarrow Ar^+ + Ar_m^*$
H-atom transfer	$Ar^+ + H_2 \rightarrow ArH^+ + H$
Asymmetric charge transfer	$Ar^+ + H_2 \rightarrow$ fast Ar + H_2^+
ArH^+ Monte Carlo model—	
Elastic scattering	$ArH^+ + Ar \rightarrow ArH^+ +$ fast Ar
Collision-induced dissociation	$ArH^+ + Ar \rightarrow$ fast Ar + $H^+ + Ar$
Collision-induced dissociation	$ArH^+ + Ar \rightarrow$ fast $Ar^+ + H + Ar$
Elastic scattering	$ArH^+ + H_2 \rightarrow ArH^+ +$ fast H_2
Proton transfer	$ArH^+ + H_2 \rightarrow$ fast Ar + H_3^+
H^+ Monte Carlo model—	
Elastic scattering	$H^+ + Ar \rightarrow H^+ +$ fast Ar
Asymmetric charge transfer	$H^+ + Ar \rightarrow$ fast H + Ar^+
Symmetric charge transfer	$H^+ + H \rightarrow$ fast H + H^+
Total vibrational excitation	$H^+ + H_2 \rightarrow H^+ + H_2^*$ (v)
Elastic scattering	$H^+ + H_2 \rightarrow H^+ +$ fast H_2
Asymmetric charge transfer	$H^+ + H_2 \rightarrow$ fast H + H_2^+
H_2^+ Monte Carlo model—	
Proton transfer	$H_2^+ + Ar \rightarrow H + ArH^+$
Asymmetric charge transfer	$H_2^+ + Ar \rightarrow$ fast H_2 + Ar^+
Proton transfer	$H_2^+ + H_2 \rightarrow H + H_3^+$
Symmetric charge transfer	$H_2^+ + H_2 \rightarrow$ fast H_2 + H_2^+
H_3^+ Monte Carlo model—	
Elastic scattering	$H_3^+ + Ar \rightarrow H_3^+ +$ fast Ar
Proton transfer	$H_3^+ + Ar \rightarrow$ fast H_2 + slow ArH^+
Charge transfer + dissociation	$H_3^+ + Ar \rightarrow$ fast H_2 + fast H + slow Ar^+
Collision-induced dissociation	$H_3^+ + Ar \rightarrow$ fast H^+ + fast H_2 + slow Ar
Collision-induced dissociation	$H_3^+ + Ar \rightarrow$ fast H_2^+ + fast H + slow Ar
Elastic scattering	$H_3^+ + H_2 \rightarrow H_3^+ +$ fast H_2
Proton transfer	$H_3^+ + H_2 \rightarrow$ fast H_2 + slow H_3^+
Proton transfer + dissociation	$H_3^+ + H_2 \rightarrow$ fast H_2 + slow H_2 + slow H^+
Proton transfer + dissociation	$H_3^+ + H_2 \rightarrow$ fast H_2 + slow H + slow H_2^+
Charge transfer + dissociation	$H_3^+ + H_2 \rightarrow$ fast H_2 + fast H + slow H_2^+
Collision-induced dissociation	$H_3^+ + H_2 \rightarrow$ fast H_2^+ + fast H + slow H_2
Collision-induced dissociation	$H_3^+ + H_2 \rightarrow$ fast H^+ + fast H_2 + slow H_2
Collision-induced dissociation	$H_3^+ + H_2 \rightarrow$ fast H^+ + 2 fast H + slow H_2
Fast Ar^0 Monte Carlo model—	
Elastic scattering	fast Ar + slow Ar $\rightarrow$ fast Ar + fast Ar
Ionization	fast Ar + slow Ar $\rightarrow$ fast Ar + $Ar^+ + e^-$
Excitation to the metastable levels	fast Ar + slow Ar $\rightarrow$ fast Ar + Ar_m^*

The three models are also combined with the models for the other plasma species, and the entire modeling network is solved iteratively (*i.e.*, the output of one model is used as input in the other models) until final convergence is reached.

3 Results and discussion

3.1 Electrical conditions

The two-dimensional modeling network was applied to a cylindrically symmetrical glow discharge cell used in the VG9000 glow discharge mass spectrometer for the analysis of flat samples (see, for example, refs. 38 and 39). The glow discharge conditions under study were a discharge voltage of 1000 V, and a gas pressure and temperature of 75 Pa and 330 K. The corresponding electrical current was calculated (based on the fluxes of the charged plasma species) to be of the order of 1–2 mA and decreased at increasing hydrogen addition (Fig. 1). The reasons for this drop in electrical current are the lower electron and Ar^+ ion fluxes, which are not fully compensated by the rise in fluxes of the other charged species playing a role in the argon–hydrogen discharge (*i.e.*, the hydrogen-related ions). As is apparent from Fig. 1, the electrical current does not drop linearly, but more or less exponentially as a function of hydrogen addition, which means that the effect of the hydrogen addition is most pronounced at low hydrogen concentrations ($\leqslant$ 1%).

3.2 Electron and Ar^+ ion densities

Fig. 2 illustrates the calculated one-dimensional density profiles of (a) the electrons and (b) the Ar^+ ions for various argon–hydrogen mixtures (ranging from 0 to 10% hydrogen). Our

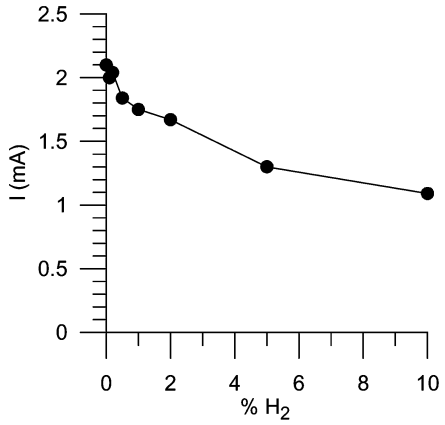

Fig. 1 Calculated electrical current as a function of hydrogen addition, for the VG9000 glow discharge flat cell with about 1 cm length and 1.25 cm radius, at a voltage of 1000 V and a gas pressure and temperature of 75 Pa and 330 K.

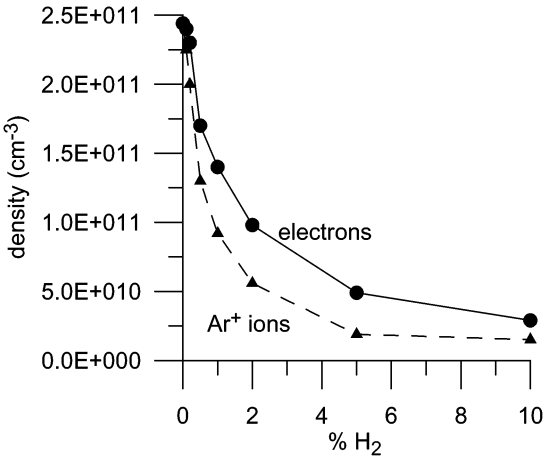

Fig. 3 Calculated densities of the electrons (solid line) and Ar^+ ions (dashed line) at the maximum of their profiles as a function of hydrogen addition and under the same discharge conditions as in Fig. 1.

calculations predict that the density profiles of these species will drop with increasing hydrogen addition. The effect is already visible at the very small hydrogen concentration of 0.1%, but becomes especially pronounced at hydrogen additions of 0.5% and more. This drop can be explained by the reactions taken into account in the model.[34] For the electrons, it was found that no additional production mechanisms play a significant role in the argon–hydrogen discharge compared with the pure argon discharge. However, for the loss of species, there are some extra important loss mechanisms in the argon–hydrogen discharge. Indeed, in the pure argon discharge, the loss of electrons is almost exclusively caused by diffusion to the walls and subsequent recombination at the walls, because electron–Ar^+ ion recombination in the plasma is not important (due to the low rate coefficient). In the argon–hydrogen discharge, on the other hand, electron recombination with ArH^+ and H_3^+ ions plays an important role (because the rate coefficients for dissociative recombination with molecular ions are significantly higher), which explains the drop in electron density.[34]

The drop in Ar^+ ion density as a function of hydrogen addition is also caused by additional important loss mechanisms in the argon–hydrogen discharge and the absence of additional significant production mechanisms. Indeed, in the pure argon discharge, the dominant loss is by diffusion and recombination at the walls, whereas in the argon–hydrogen discharge, charge transfer and especially H-atom transfer between Ar^+ ions and H_2 molecules (giving rise to H_2^+ and ArH^+ ions, respectively) cause an additional drop in the Ar^+ ion density.[34]

The drop in electron and Ar^+ ion densities can be seen clearly in Fig. 3, where the densities at the maximum of their profiles are plotted as a function of increasing H_2 addition. It is clear that the drop in density is most pronounced at low H_2 addition, and is even more significant for the Ar^+ ions than for the electrons, especially at low H_2 concentration. Indeed, the electron density should be equal to the total ion density in the bulk plasma, and (at least for low H_2 addition) a rise in the other ion densities is observed (see below), which explains the somewhat slower drop in the electron density at low H_2 addition compared to the Ar^+ ion density.

3.3 ArH^+, H^+, H_2^+ and H_3^+ ion densities

Fig. 4 presents the one-dimensional density profiles of the hydrogen-related ions, *i.e.*, ArH^+ (a), H^+ (b), H_2^+ (c) and H_3^+ (d), at several different H_2 concentrations. All these ionic species are characterized by more or less the same qualitative density profile as the Ar^+ ions, *i.e.*, with low values in the CDS and a maximum in the NG at about 0.6 cm from the cathode. It is clear that the ArH^+ and H_3^+ ions have a rather high density, which is on average only about one order of magnitude lower than the Ar^+ ion density, whereas the H^+ and H_2^+ ions have much lower densities, which can be considered to be negligible in the argon–hydrogen discharge under the conditions in this study. In general, the densities of these four ionic species first increase with hydrogen addition and then decrease as the hydrogen concentration rises above 1–2%.

This behavior is more clearly illustrated in Fig. 5, which

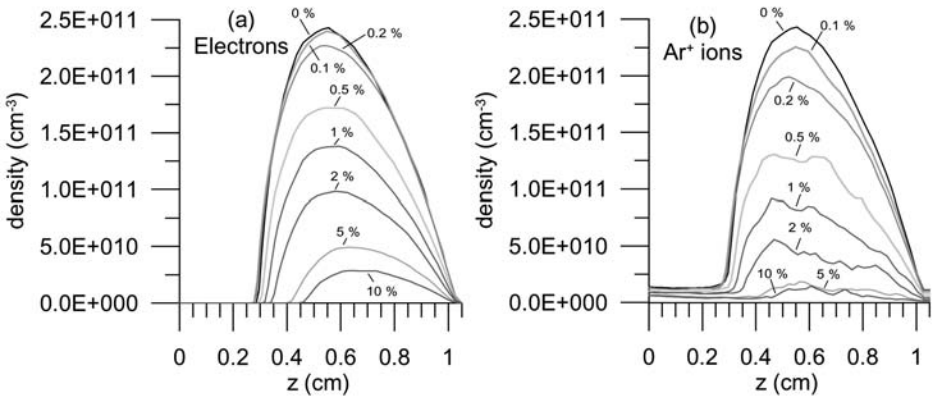

Fig. 2 Calculated one-dimensional density profiles of the electrons (a) and the Ar^+ ions (b) at various hydrogen concentrations and under the same discharge conditions as in Fig. 1.

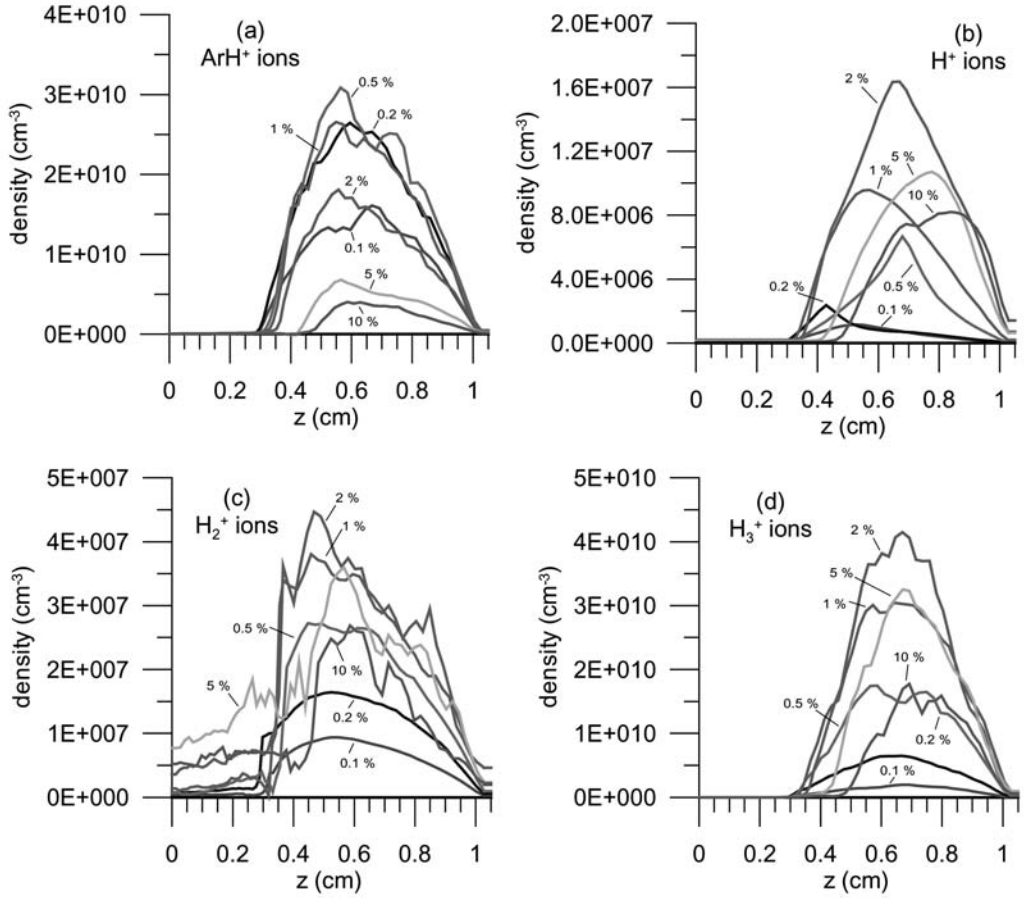

Fig. 4 Calculated one-dimensional density profiles of the ArH^+ ions (a), H^+ ions (b), H_2^+ ions (c) and H_3^+ ions (d) at various hydrogen concentrations and under the same discharge conditions as in Fig. 1.

shows the ion densities at the maximum of their profile as a function of hydrogen addition. The ArH^+ density first rises significantly up to a hydrogen concentration of about 0.5%. At this moment, the ArH^+ density at the maximum is about 3×10^{10} cm^{-3}, which is only a factor of 4 lower than the Ar^+ ion density at the maximum of its profile, calculated for this condition. At higher H_2 concentrations, the ArH^+ ion density drops in a similar way to the Ar^+ ion density. The reason for this behavior can be found again in the production and loss mechanisms of the ArH^+ ions.[34] Indeed, the dominant production is a transfer of H atoms between Ar^+ ions and H_2 molecules. On one hand, the H_2 concentration increases, but, on the other hand, the Ar^+ ion density decreases, so that the production appears to reach a maximum as a function of hydrogen addition. Moreover, the most important loss mechanism, especially at high H_2 concentrations, is proton transfer between ArH^+ and H_2, which also explains the drop in ArH^+ ion density at sufficiently high hydrogen concentrations.

The H^+, H_2^+ and H_3^+ ion densities reach a maximum and then diminish with increasing hydrogen addition, but the maximum is found at somewhat higher hydrogen concentrations (typically about 2%; see Fig. 5). This behavior is at first sight a bit unexpected, because it appears logical that the H^+, H_2^+ and H_3^+ ions increase in density with rising hydrogen addition. However, this behavior can be explained again based on the production and loss mechanisms.[34] Indeed, the H_3^+ ions are primarily formed by proton transfer between ArH^+ ions and H_2 molecules. At low rates of hydrogen addition, both ArH^+ and H_2 densities increase, leading to a rise in H_3^+ ion density. However, at hydrogen concentrations of 0.5% and more, the ArH^+ density drops. At first, the rising H_2 density still causes an increase in H_3^+ ion density, but above about 2% hydrogen addition the drop in ArH^+ density dominates above the rise in H_2 density, explaining the further drop in H_3^+ ion density. It is worthwhile to mention that, at a hydrogen concentration of 2%, the maximum H_3^+ ion density is calculated to be above 4×10^{10} cm^{-3}, which is only slightly lower than the calculated Ar^+ ion density for this condition (*ca.* 5×10^{10} cm^{-3}). As far as the H^+ ions are concerned, they are primarily formed by collision-induced dissociation of H_3^+ ions by Ar atoms and, hence, the behavior of H^+ ion density follows logically more or less the H_3^+ ion density behavior as a function of hydrogen addition. Finally, H_2^+ ions are mainly created by a charge transfer between Ar^+ ions and H_2

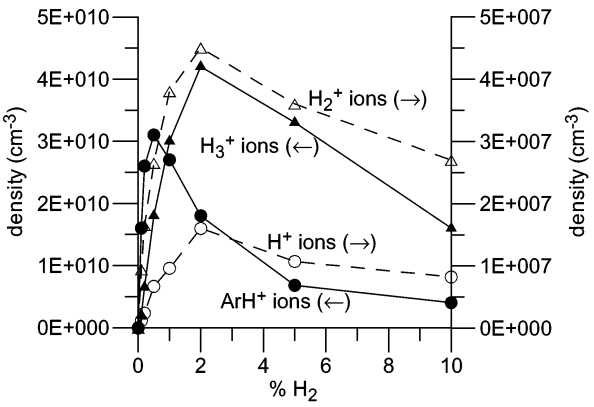

Fig. 5 Calculated densities of the ArH^+ and H_3^+ ions (solid lines, left axis) and of the H^+ and H_2^+ ions (dashed lines, right axis) at the maximum of their profiles as a function of hydrogen addition and under the same discharge conditions as in Fig. 1.

molecules, and their behavior as a function of hydrogen addition is again a combination of the decreasing Ar^+ ion density and the rising H_2 density.

3.4 H atom and H_2 molecule densities

The calculated one-dimensional density profiles of the H atoms and H_2 molecules, at the different argon–hydrogen mixtures under study, are depicted in Fig. 6 (a and b). As expected, the densities of these species increase with hydrogen addition. The density of the H_2 molecules (see Fig. 6a) appears to be constant in space, and equal to the initial H_2 density given as input in the model, in spite of the fact that a large number of production and loss processes were taken into account in the H–H_2 fluid model.[34] The H_2 density is therefore equal to the percentage of hydrogen multiplied by the gas density calculated from the ideal gas law (see above). Hence, the H_2 density increases linearly with the percentage of hydrogen, as appears also from Fig. 7. It is worth mentioning here that the total gas density (argon + hydrogen) at the gas pressure and temperature of 75 Pa and 330 K is calculated to be 1.65×10^{16} cm^{-3}.

The calculated H atom density is not constant in space, but reaches a maximum at about 1–2 mm from the cathode (see Fig. 6b). The reason for this position of the maximum is that the most important production mechanism of the H atoms is dissociative excitation of H_2 molecules by argon metastable atoms, and the latter also reach their maximum at 1–2 mm from the cathode (see below). The H atom density does not increase proportionally with the H_2 concentration, as appears from Fig. 6b and Fig. 7. Indeed, at low H_2 concentrations (up to about 2%), the H atom density increases much faster than the H_2 molecule density, whereas, at higher H_2 concentrations, the opposite trend is observed. The reason is again found in the production of H atoms from dissociative excitation of H_2 molecules by argon metastable atoms, because the latter species, and hence this production rate, are becoming less important at high H_2 concentrations (see below).

From the calculated H atom and H_2 molecule densities, the degree of dissociation of hydrogen can be obtained. As is apparent from Fig. 8, the degree of H_2 dissociation decreases more or less exponentially as a function of hydrogen concentration. At the high H_2 concentration of 10%, the degree of dissociation is calculated to be of the order of 10^{-5}, whereas this value increases to about 5×10^{-4} at the low hydrogen concentration of 0.1%. Keeping in mind that the degree of ionization of argon was calculated to be typically 10^{-5}–10^{-6} under the conditions in this study,[38] the degree of H_2 dissociation is comparable to the degree of argon ionization at high H_2 concentrations (10% and higher), whereas it becomes significantly higher at low H_2 concentrations. Nevertheless, Figs. 6, 7 and 8 suggest that, under these conditions, the added hydrogen is primarily present in molecular form in the argon–hydrogen glow discharge plasma. In ref. 33, a preliminary estimate of the degree of dissociation in analytical glow discharges for argon with 1% H_2 were given and, for the similar conditions as in this study, somewhat higher values (of the order of 5%) were estimated. Hence, this value was too high, which is not unexpected, since it was only obtained from

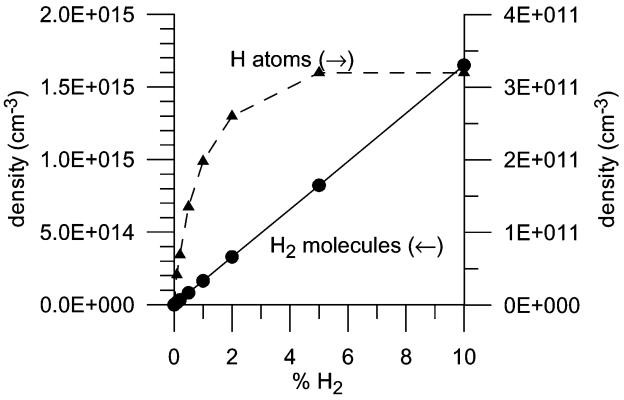

Fig. 7 Calculated densities of H_2 molecules (solid line, left axis) and H atoms (dashed line, right axis) at the maximum of their profiles as a function of hydrogen addition and under the same discharge conditions as in Fig. 1.

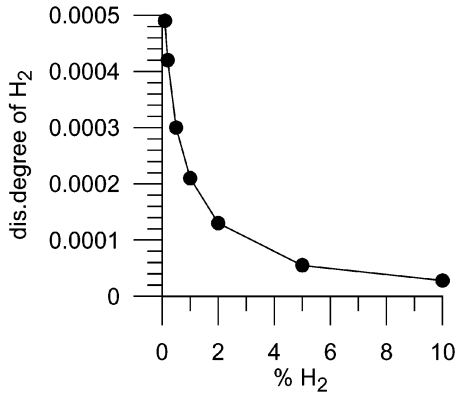

Fig. 8 Calculated degree of dissociation of H_2 as a function of hydrogen addition and under the same discharge conditions as in Fig. 1.

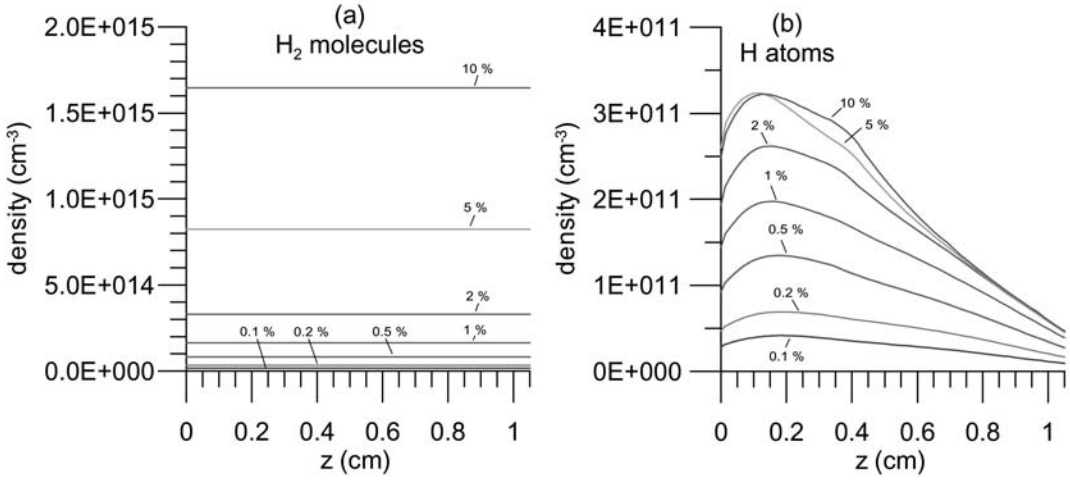

Fig. 6 Calculated one-dimensional density profiles of H_2 molecules (a) and H atoms (b) at various hydrogen concentrations and under the same discharge conditions as in Fig. 1.

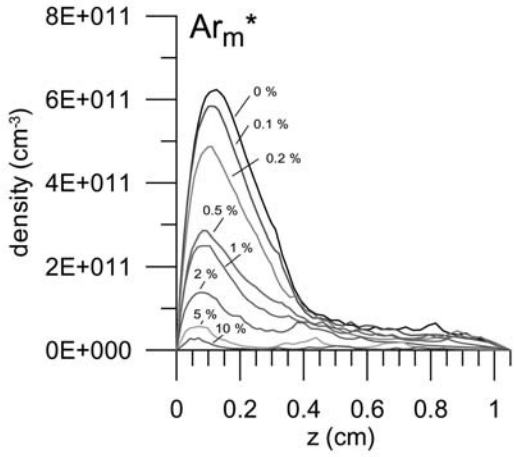

Fig. 9 Calculated one-dimensional density profiles of the argon metastable atoms (Ar_m*) at various hydrogen concentrations and under the same discharge conditions as in Fig. 1.

preliminary estimates. It shows that full modeling is required to produce quantitative numbers of plasma quantities.

3.5 Argon metastable atom density

Fig. 9 illustrates the calculated one-dimensional argon metastable atom (Ar_m*) density profiles at various hydrogen concentrations. As was already mentioned above, the argon metastable density reaches a maximum at about 1–2 mm from the cathode, and drops significantly at increasing hydrogen concentrations. The pronounced maximum close to the cathode is attributed to the dominant production of metastable argon atoms by fast argon ion and atom impact excitation, which is important near the cathode (where the ions and atoms reach high enough energies for excitation).[35] The drop in argon metastable atom density at increasing hydrogen concentrations (see also Fig. 10) is explained by the quenching of argon metastable atoms due to H_2 molecules (*i.e.*, dissociative excitation of H_2 molecules to form H atoms; see above). This is, indeed, found to be an important loss mechanism of the argon metastable atoms in the argon–hydrogen discharge (with a calculated contribution ranging from about 10% at 0.1% hydrogen to almost 80% at 10% hydrogen added to the discharge).

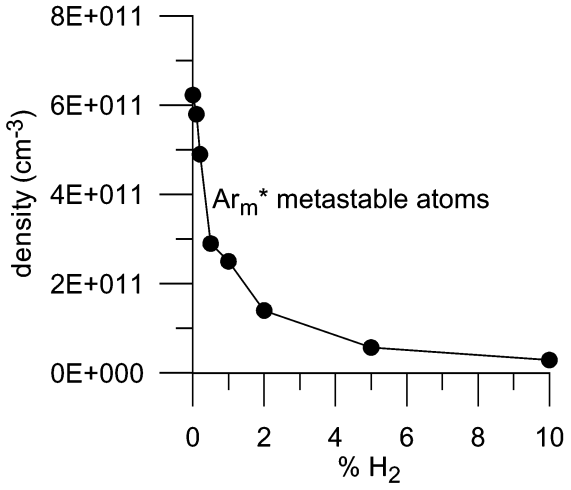

Fig. 10 Calculated Ar_m* density at the maximum of its profile as a function of hydrogen addition and under the same discharge conditions as in Fig. 1.

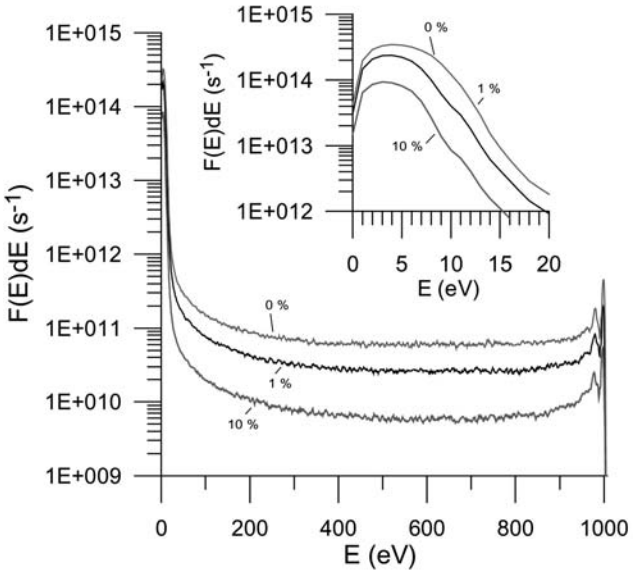

Fig. 11 Calculated electron energy distribution functions (EEDF) at the interface between CDS and NG, at various hydrogen concentrations and under the same discharge conditions as in Fig. 1.

3.6 Electron energy distribution function

Because it has been reported in the literature that the addition of hydrogen can alter the electron energy distribution function (EEDF) in an argon–hydrogen rf discharge,[40] we investigated whether this effect occurs also for the glow discharge under study here. Fig. 11 shows the calculated EEDF in a pure argon discharge and an argon–hydrogen discharge with 1% hydrogen and with 10% hydrogen, expressed in terms of flux and taken at the interface between the CDS and NG. For the sake of clarity, the intermediate hydrogen concentrations studied in this work are not presented here, but the trend observed in Fig. 11 applies also to the other hydrogen concentrations.

The EEDF appear to be very similar at the different hydrogen concentrations under study, with most electrons present at energies below 10 eV (see inset figure) and with a long tail that extends in the form of a plateau up to energies of 1000 eV (*i.e.*, corresponding to the applied discharge voltage). At 1000 eV, a minor peak is observed, which corresponds to electrons that have traversed the entire CDS without any collisions. Because of the presence of these high-energy electrons, the average electron energy at the end of the CDS is quite high, *i.e.*, typically 450 eV under the conditions in this study. It should be mentioned that this average energy value is calculated from the flux; the average energy based on density would be much lower (because of the higher contribution of low energy electrons). In the NG, the energy value will drop, because the electrons will no longer gain much energy from the weak electric field and they will lose their energy more efficiently by collisions. It is important to note that the electron energy was calculated to be very similar for all hydrogen concentrations under study. Hence, the addition of hydrogen does not appear to affect the electron energy. This is in contrast to the results reported in ref. 40, where a deviation from the Maxwell distribution, typically encountered in the pure argon rf discharge under the conditions in that work, was observed with the addition of hydrogen. More specifically, the electrons with energies between 2 and 10 eV were shifted to a lower energy (below 2 eV) as a result of vibrational excitations. However, the EEDF reported in ref. 40 were measured in an rf discharge typically used for technological applications (which operates at much lower voltages) and in the middle of the plasma where the electric field is too weak to heat the electrons, in order to

compensate for the energy loss by vibrational excitations. In our case, the electrons were accelerated significantly by the strong electric field in the CDS, and the effect of vibrational excitation of hydrogen on the EEDF appeared to be negligible.

The only difference in the EEDF calculated for different argon–hydrogen mixtures are in the absolute values, as is clear from Fig. 11. Indeed, the EEDF are presented as flux energy distributions and the total electron flux in the pure argon discharge is somewhat higher than when 1% or 10% hydrogen is added. This was expected from the effect of hydrogen on the electrical current and on the electron density (see Figs. 1, 2a and 3).

3.7 Energy distribution functions of the various ions and the fast Ar^0 atoms

We also investigated the effect of hydrogen on the energy distribution functions (EDF) of the various ions and the fast Ar^0 atoms. Fig. 12 illustrates the calculated EDF, expressed again in terms of flux, of Ar^+ ions (a), fast Ar^0 atoms (b), ArH^+ ions (c), H^+ ions (d), H_2^+ ions (e) and H_3^+ ions (f), when bombarding the cathode ($z = 0$ cm). Again, only the calculated results for three different hydrogen concentrations are presented, *i.e.*, at 0.1% (which gives similar values as the pure argon discharge), at 1% and at 10% hydrogen, in order not to unnecessarily complicate the figures. The Ar^+ ions are characterized by an exponentially decreasing EDF toward high energies (linear decrease on a logarithmic scale; see Fig. 12(a)). The reason is that the Ar^+ ions lose their energy quite efficiently by elastic collisions (including charge transfer) with argon atoms, so that most Ar^+ ions have rather low energies when arriving at the cathode. The EDF of the fast Ar^0 atoms (Fig. 12(b)) exhibits also a decreasing behavior as a function of energy, and the drop is even more pronounced than for the Ar^+ ions. Indeed, the fast Ar^0 atoms are primarily created from

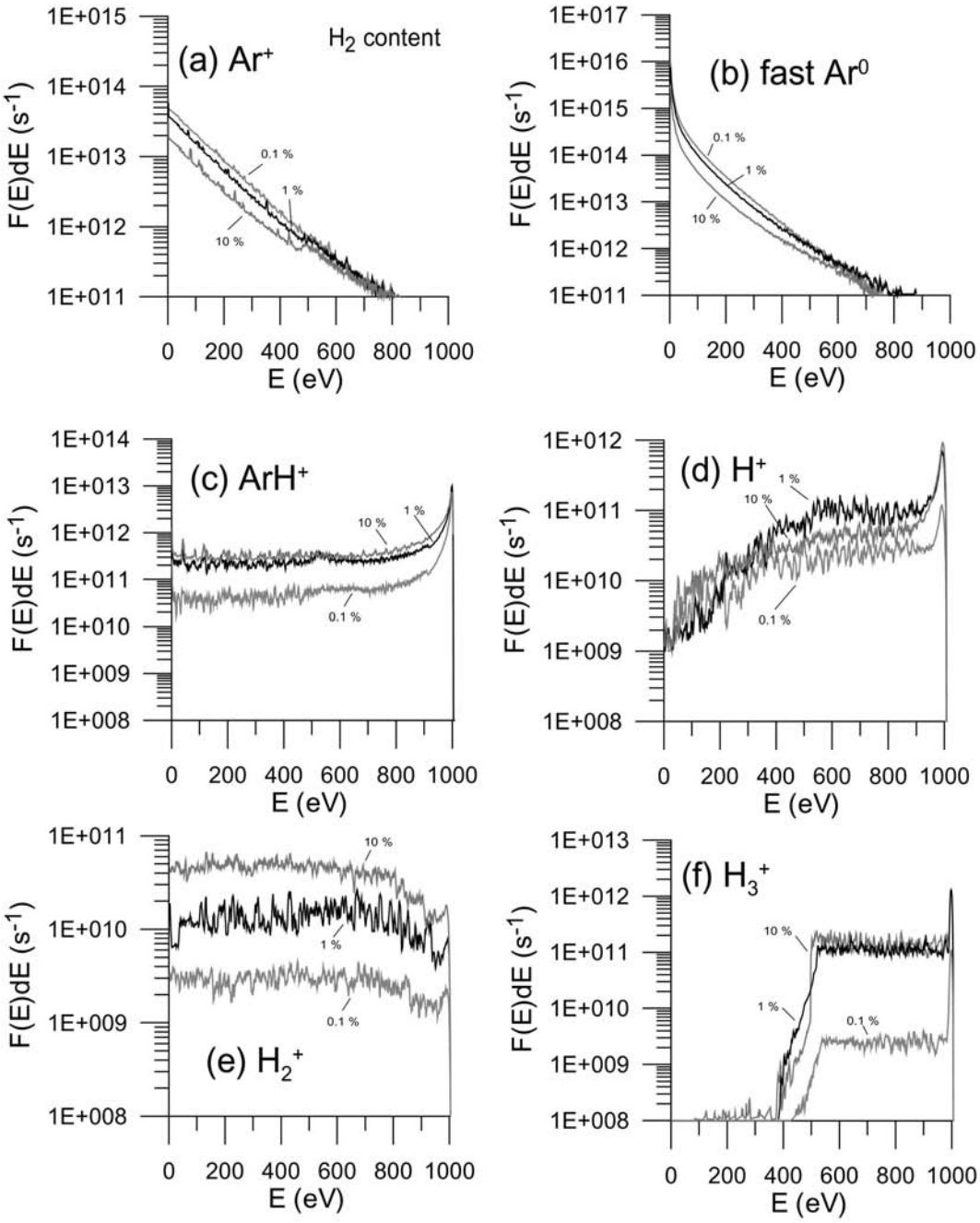

Fig. 12 Calculated energy distribution functions (EDF) of Ar^+ ions (a), fast Ar^0 atoms (b), ArH^+ ions (c), H^+ ions (d), H_2^+ ions (e) and H_3^+ ions (f) bombarding the cathode, at various hydrogen concentrations and under the same discharge conditions as in Fig. 1.

energy transfer to the argon gas in collisions of Ar^+ ions, and their energy cannot therefore be higher than the typical Ar^+ ion energy. Moreover, in contrast to the ionic species, the fast Ar^0 atoms are no longer accelerated by the electric field in the CDS on their way towards the cathode; they only lose their energy further by elastic collisions with the argon gas atoms. Consequently, their energy is typically lower than the Ar^+ ion energy when bombarding the cathode. On the other hand, it is important to realize that the flux of fast Ar^0 atoms bombarding the cathode is considerably higher than the Ar^+ ion flux, because a large number of fast Ar^0 atoms are created in the CDS through elastic collisions with argon gas atoms and even by collisions with other fast Ar^0 atoms. Indeed, the total Ar^+ ion flux at the cathode is calculated to be of the order of 5×10^{15}–10^{16} cm^{-2} s^{-1} (depending on the hydrogen concentration), whereas the total fast Ar^0 atom flux is of the order of 1–3 $\times$ 10^{17} cm^{-2} s^{-1}. Hence, it is expected that the fast Ar^0 atoms will play an important role in the cathode sputtering process (see below).

The ArH^+ ions are characterized by a completely different EDF, with a plateau value over almost the entire energy range and a maximum at 1000 eV (which corresponds to the applied discharge voltage). Hence, this indicates that the ArH^+ ions lose less energy by collisions in the CDS on their way towards the cathode, and that a large fraction of the ArH^+ ions travel through the CDS without any collisions. It should be mentioned that a very important collision process for the ArH^+ ions is proton transfer with H_2 molecules, giving rise to the formation of H_3^+ ions and fast Ar atoms (see Table 2 and the cross sections presented in ref. 34). This collision mechanism does not result in a lowering of the ArH^+ energy, but does result in the loss of ArH^+ ions and the creation of other species. The effect of this collision mechanism is therefore not observable in the shape of the EDF of ArH^+ ions. This affects only the absolute values, *i.e.*, the flux of ArH^+ ions bombarding the cathode, which is clearly lower than the Ar^+ ion flux (typically ranging from 2×10^{14} to 2×10^{15} cm^{-2} s^{-1}, depending again on the hydrogen concentration).

The H^+, H_2^+ and H_3^+ ions also exhibit a more or less similar EDF to the ArH^+ ions, as appears from the calculation results presented in Fig. 12 [(d), (e) and (f)], with a plateau-like behavior over most of the energy range and a peak at maximum energy (at least in the case of the H^+ and H_3^+ ions). The fluctuations in the EDF are due to statistical problems. The EDF behavior suggests that these species again do not lose their energy as efficiently by collisions in the CDS, as compared with the Ar^+ ions. On the other hand, and analogously to the behavior of the ArH^+ ions, they are subject to chemical reaction collisions, resulting in destruction of these species and the formation of other species. This is especially true for the H_3^+ ions, which explains their low flux when bombarding the cathode in contrast to their relatively high density in the NG (see Fig. 4(d)). The total fluxes of the H^+, H_2^+ and H_3^+ ions at the cathode are calculated to be in the range from 10^{13}–4×10^{14} cm^{-2} s^{-1} (depending again on the hydrogen concentration, see below).

For all these ionic species, as well as for the fast Ar^0 atoms, it is clear that the addition of hydrogen has no major effect on the shape of the EDF and, therefore, on the average energies of the various species, which is analogous to the effect on the electron behavior. The average energies were calculated to be around 100 eV for the Ar^+ ions, about 25 eV for the fast Ar^0 atoms, of the order of 800 eV for the ArH^+ ions, about 650 eV for the H^+ ions, about 250 eV for the H_2^+ ions and about 900 eV for the H_3^+ ions.

On the other hand, adding hydrogen to the argon discharge has some effect on the absolute values of the EDF, *i.e.*, on the fluxes of the ionic species and fast Ar^0 atoms bombarding the cathode, as appears from Fig. 12. As expected from above, the absolute values of the EDF of Ar^+ ions and fast Ar^0 atoms decrease slightly when hydrogen is added to the argon discharge, whereas the EDF of the ArH^+, H^+, H_2^+ and H_3^+ ions slightly increase in absolute values with rising hydrogen concentration.

3.8 Sputtering of the copper cathode

From the last observation, it is expected that the relative contribution of the hydrogen-related species to the cathode sputtering will increase with the addition of more and more hydrogen to the argon discharge. Fig. 13 shows the calculated relative contributions to the sputtering of the fast Ar^0 atoms, the Ar^+ and ArH^+ ions (solid lines, left axis), and of the H^+, H_2^+ and H_3^+ ions (broken lines, right axis). It is clear that the fast Ar^0 atoms play a dominant role in the sputtering. Their contribution is around 80% in a pure argon discharge and drops gradually to values of about 65% at hydrogen concentrations of 5–10%. This drop is due to the increasing importance of ArH^+ ions to the sputtering process. Indeed, its relative contribution rises from 0 in a pure argon discharge, to a few % at hydrogen additions of less than 1%, and finally to about 16% at hydrogen concentrations of 5–10%. The last contribution is almost as high as the contribution of Ar^+ ions, which is around 18% (more or less constant for all hydrogen additions investigated). Hence, in spite of the lower ArH^+ flux bombarding the cathode (2×10^{14}–2×10^{15} cm^{-2} s^{-1}, depending on the hydrogen concentration, compared to 5×10^{15}–10^{16} cm^{-2} s^{-1} for Ar^+ ions), the ArH^+ ions play a significant role in the sputtering process. The reason is that they are characterized by a higher energy and the sputtering efficiency rises with the energy of the bombarding species in the energy range of interest here.[41] This phenomenon of higher kinetic energy of ArH^+ ions compared to Ar^+ ions when bombarding the cathode, and hence the important role of ArH^+ ions to sputtering in an argon–hydrogen discharge, has been reported in the literature.[15] It was even found[15] that, for certain conditions, the sputter rates can reach a maximum at 5–20% hydrogen added to the argon discharge.

As far as the other three hydrogen-related ions (H^+, H_2^+ and H_3^+) are concerned, it appears from Fig. 13 (broken lines, right axis) that their contribution to sputtering also increases when more hydrogen is added to the discharge, but remains of minor importance compared to the role of fast Ar^0 atoms, Ar^+ ions and ArH^+ ions, *i.e.*, at a maximum at about 0.25% for H_3^+, 0.09% for H_2^+ and 0.07% for the H^+ ions, as was already expected from their low fluxes when bombarding the cathode in combination with their low sputtering efficiency (due to their low mass).

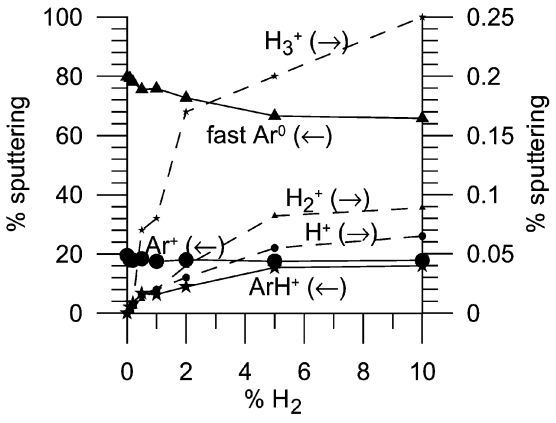

Fig. 13 Calculated relative contributions to the cathode sputtering process by fast Ar^0 atoms, Ar^+ ions and ArH^+ ions (solid lines, left axis) and by H_3^+, H_2^+ and H^+ ions (dashed lines, right axis) as a function of hydrogen addition and under the same discharge conditions as in Fig. 1.

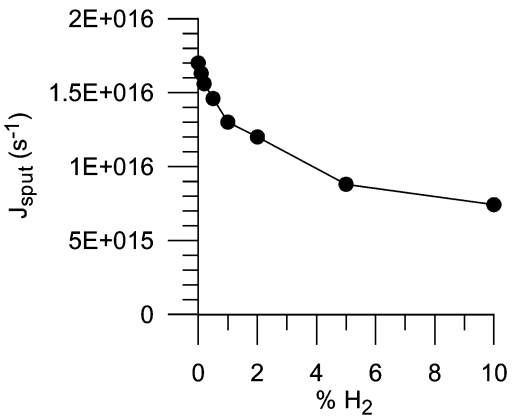

Fig. 14 Calculated sputtering flux at the copper cathode as a function of hydrogen addition and under the same discharge conditions as in Fig. 1.

Finally, it should be mentioned that the Cu^+ ions also play a role in the sputtering process of the copper cathode (*i.e.*, so-called self-sputtering). The flux of Cu^+ ions bombarding the cathode is typically several orders of magnitude lower than the Ar^+ ion flux, but the Cu^+ ion EDF is characterized by a pronounced peak at maximum energy.[37] Therefore, the relative contribution of Cu^+ ions to sputtering is calculated to be of the order of 0.6% in the pure argon discharge for the conditions under study here. This contribution drops, however, to values of about 0.02% when 10% hydrogen is added to the discharge, due to the decreasing role of Cu^+ ions in the discharge (see below).

The total sputtering flux, as a result of the bombardment of all the above-mentioned species, is plotted *versus* hydrogen addition in Fig. 14. It appears that, in spite of the growing importance of the hydrogen-related species to sputtering (especially the ArH^+ ions), the total sputtering flux decreases with rising hydrogen concentration. This is in contrast to the results reported in ref. 15 (see above), where a maximum sputtering rate was observed for 5–20% hydrogen addition. The reason is, of course, that under the conditions in this study (more specifically the high voltage of 1000 V), the fast Ar^0 atoms play the dominant role in sputtering, even at the highest hydrogen addition investigated. The drop in sputtering flux is explained by this decrease in flux with rising hydrogen concentration, as presented in Fig. 14.

3.9 Sputtered Cu atom and Cu^+ ion densities

As a result of the lower sputtering flux, the sputtered Cu atom and Cu^+ ion densities also drop at increasing hydrogen concentrations, as is illustrated in Figs. 15(a), 15(b) and 16. The Cu atom density reaches a maximum at about 1–2 mm from the cathode for all hydrogen additions investigated (see Fig. 15(a)). It drops at a similar rate as the sputtering flux (*cf.*, Figs. 14 and 16). For 1% hydrogen added, the Cu atom density drops by a factor of 1.6, whereas, at 10% hydrogen added, the drop is somewhat more than a factor of 3.

The Cu^+ ion density is low and more or less constant in the CDS and reaches a maximum in the NG about halfway along the discharge, in analogy with the density profiles of Ar^+ and other ions (see above). It drops more rapidly as a function of hydrogen concentration, as is clear from Fig. 16 (broken line, right axis). Indeed, it drops by a factor of more than 3 at 1% hydrogen added and by almost two orders of magnitude when 10% hydrogen is added to the argon discharge. This result, although following logically from our calculations (see also below), is in contrast to the observations in a fast flowing argon–hydrogen glow discharge,[7] where the addition of hydrogen resulted in a drop in Ar^+ ion intensity and an increase in Cu^+ ion intensity in the mass spectrum. However, the experimental results of ref. 7 are probably more complicated than simply being the result of the addition of hydrogen, because of the effect of the fast gas flow.

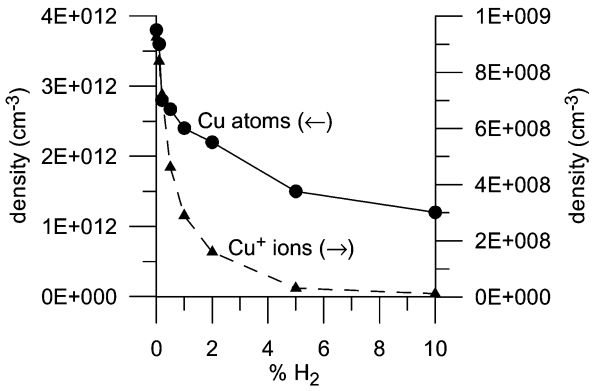

Fig. 16 Calculated densities of Cu atoms (solid line, left axis) and Cu^+ ions (broken line, right axis) at the maximum of their profiles as a function of hydrogen addition and under the same discharge conditions as in Fig. 1.

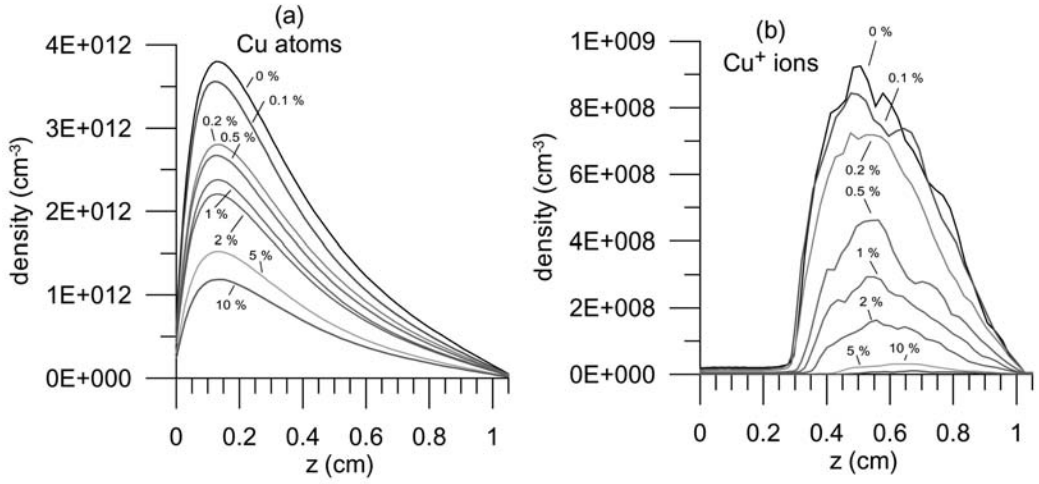

Fig. 15 Calculated one-dimensional density profiles of sputtered Cu atoms (a) and the corresponding Cu^+ ions (b) at various hydrogen concentrations and under the same discharge conditions as in Fig. 1.

3.10 Ionization of Cu atoms

The reason for the more pronounced drop in the calculated Cu^+ ion density compared with the Cu atom density at increasing hydrogen concentrations is attributed to the decrease in efficiency of ionization of the Cu atoms in the model. Indeed, both the Ar^+ ion density and especially the Ar_m* density drop considerably when adding hydrogen to the discharge (see above, Figs. 2(b), 3, 9 and 10). Hence, asymmetric charge transfer with Ar^+ ions and especially Penning ionization by argon metastable atoms, which are generally the two most important ionization mechanisms of sputtered Cu atoms,[35,37] become less important. Electron impact ionization becomes also slightly less important, because of the somewhat lower electron flux (see Fig. 11), but the effect is less pronounced than for Penning ionization and asymmetric charge transfer. Hence, looking at the relative contributions of the three ionization mechanisms of the sputtered Cu atoms (presented in Fig. 17, integrated over the entire discharge), it is apparent that Penning ionization becomes less important as an ionization mechanism with a contribution ranging from about 70% in a pure argon discharge to roughly 40% when 10% hydrogen is added. The relative contribution of asymmetric charge transfer appears to be rather constant (with a typical value between 20 and 30%), whereas the contribution of electron impact ionization rises from about 4% in the pure argon discharge to almost 30% at a hydrogen concentration of 10%. It should be mentioned that these relative contributions are only approximate values, since the rate coefficients of Penning ionization and especially of asymmetric charge transfer are subject to considerable uncertainty. Nevertheless, the trend of increasing relative importance of electron impact ionization is expected to be a correct prediction.

The last result might explain an observation in the literature[1,2] that a better correlation could be obtained between measured relative sensitivity factors in GDMS and values predicted by simple empirical equilibrium models. The latter models are based on the first ionization potential of the elements, which determines only the cross section of electron impact ionization. Indeed, Penning ionization occurs more or less non-selectively (depending only on the mass and/or radius of the elements) as long as the ionization potential of the element is below the excitation energy of the argon metastable atoms (*i.e.*, 11.55 eV), which is the case for almost all elements with the exception of nitrogen, oxygen and chlorine.[42] Asymmetric charge transfer, on the other hand, is a very selective process, which depends on the availability of suitable energy levels of the element ions that overlap closely with the Ar^+ ion ground state (or metastable level). Hence, the better correlation with model predictions based on the first ionization potential in the argon–hydrogen discharge suggests that electron impact ionization plays a much more prominent role as an ionization mechanism of the sputtered atoms in the argon–hydrogen discharge compared to a pure argon discharge. This is, at least qualitatively, in accordance with our model predictions presented in Fig. 17.

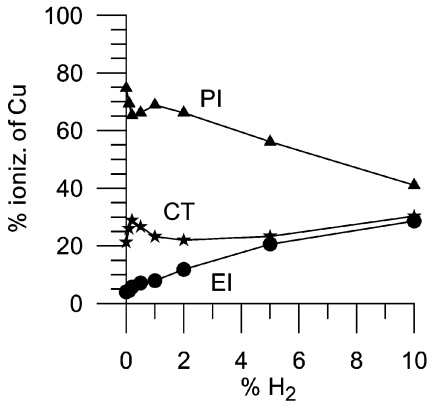

Fig. 17 Calculated relative contributions to the ionization of sputtered Cu atoms by Penning ionization with Ar_m* atoms (PI), asymmetric charge transfer with Ar^+ ions (CT) and electron impact ionization (EI), integrated over the entire discharge, as a function of hydrogen addition and under the same discharge conditions as in Fig. 1.

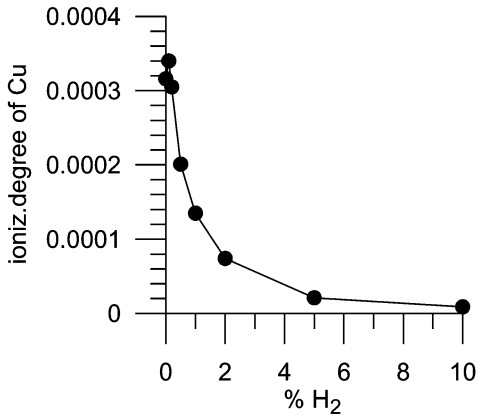

Fig. 18 Calculated degree of ionization of sputtered Cu atoms as a function of hydrogen addition and under the same discharge conditions as in Fig. 1.

Beside the changing relative contributions of the three different ionization mechanisms of the Cu atoms, the efficiency of the three ionization processes decreases in absolute terms as a function of adding hydrogen, and hence the calculated degree of ionization of Cu decreases. This is illustrated in Fig. 18. The degree of ionization is typically calculated to be somewhat above 3×10^{-4} in the pure argon discharge and at small hydrogen admixtures ($< 1\%$), and it drops to values of about 10^{-5} at hydrogen concentrations of 5–10%. When comparing Figs. 8 and 18, it becomes clear that the calculated degree of ionization of Cu and the degree of dissociation of H_2 are of the same order of magnitude and drop at a similar rate as a function of hydrogen addition. The calculated degree of ionization of argon, on the other hand, is still somewhat lower (*i.e.*, typically 10^{-5}–10^{-6} under the conditions in this study[38]).

4 Conclusion

A modeling network, consisting of several Monte Carlo and fluid models, is developed for an argon–hydrogen mixture in order to predict the effect of hydrogen added to an argon glow discharge. The plasma species considered in the model include the argon gas atoms, the electrons, fast argon atoms, argon metastable atoms, Ar^+, ArH^+, H^+, H_2^+ and H_3^+ ions, H atoms and H_2 molecules, sputtered Cu atoms and the corresponding Cu^+ ions. The hydrogen addition is varied from 0.1 to 10% and the calculation results are also compared to results obtained for a pure argon discharge. The typical operating conditions assumed for the present investigation are a discharge voltage of 1000 V and a gas pressure and temperature of 75 Pa and 330 K, which give rise to an electrical current of the order of 1–2 mA.

It is calculated that the electrical current, as well as the densities of the electrons, Ar^+ ions, argon metastable atoms, sputtered Cu atoms and Cu^+ ions, decreases considerably as a result of hydrogen addition. A drop in electron and Ar^+ ion density is also experimentally observed in the literature,[11–13] and our model predictions were able to identify the reactions responsible for these drops. The densities of the hydrogen-related ions, *i.e.*, ArH^+, H^+, H_2^+ and H_3^+, appear to pass over a maximum at a certain hydrogen concentration, which can be explained by the importance of the different production and

loss mechanisms. The densities of the H atoms and H_2 molecules, on the other hand, continue to increase with the addition of hydrogen. The effect is, however, less pronounced for the H atoms than for the H_2 molecules, resulting in a drop in the calculated degree of dissociation of H_2 with increasing hydrogen concentration.

The calculated flux energy distribution functions of electrons, various ions and fast Ar^0 atoms appear to be only affected in absolute values, *i.e.*, the fluxes of electrons, Ar^+ ions and fast Ar^0 atoms decrease, whereas the fluxes of the hydrogen-related ions increase with the addition of hydrogen. The average energy, on the other hand, of the electrons, ions and fast Ar^0 atoms remains more or less unaffected by the hydrogen concentration.

Based on the calculated flux energy distributions of the various ions and fast Ar^0 atoms bombarding the cathode, the relative contributions of these species to the sputtering process could be predicted. It was found that the fast Ar^0 atoms play a dominant role in the sputtering, although their relative contribution decreases slightly with rising hydrogen concentration, whereas the ArH^+ ions appear to gain in importance. The latter is attributed to the higher ArH^+ ion energy bombarding the cathode, in spite of the lower flux, which corresponds to observations in the literature.[15] Overall, however, the sputtering flux is calculated to decrease as a function of hydrogen concentration.

Finally, it is predicted that the degree of ionization of Cu will decrease with hydrogen addition and the relative contribution of Penning ionization will drop considerably, whereas electron impact ionization will apparently become relatively more important. The last can explain observations in the literature in which a better correlation could be reached in an argon–hydrogen discharge compared to a pure argon discharge, between measured relative sensitivity factors for GDMS and values predicted by simple empirical equilibrium models based on the first ionization potential of the elements. Indeed, the first ionization potential plays a role only in the electron impact ionization cross-section and not in the rate coefficients for Penning ionization and asymmetric charge transfer. Hence, this suggests that electron impact ionization would be more important in the argon–hydrogen discharge than in the pure argon discharge, which is, at least qualitatively, in accordance with our predictions.

It can be concluded that our model predictions can explain most of the effects observed experimentally in Ar–H_2 glow discharges. Hence, they provide a realistic picture of the role of hydrogen in glow discharges and are therefore useful for better analytical practice. The only experimental observation made in the literature for argon–hydrogen analytical glow discharges that cannot yet be predicted by our model is the fact that some optical emission lines drop in intensity, whereas other line intensities show a rise as a function of hydrogen addition. Indeed, this can only be explained by comparing in detail the energy levels of H atoms and H_2 molecules with the energy level schemes of the elements concerned, because here a selective mechanism is expected to play a role (*i.e.*, selective population or quenching of certain energy levels). We plan to perform such a study in the near future based on a systematic experimental survey.

Acknowledgement

The author is indebted to the Flemish Fund for Scientific Research (FWO-Flanders) for financial support. This research is also sponsored by the Federal Services for Scientific, Technical and Cultural Affairs of the Prime Minister's Office (DWTC/SSTC) through IUAP-IV (Conv. P4/10). The author also acknowledges A. V. Phelps for supplying input data for the model and for the many interesting discussions.

References

1 R. W. Smithwick III, D. W. Lynch and J. C. Franklin, *J. Am. Soc. Mass Spectrom.*, 1993, **4**, 278.
2 M. Saito, *Anal. Chim. Acta*, 1997, **355**, 129.
3 A. Bengtson and S. Hänström, in *Proceedings of Fifth International Conference on Progress in Analytical Chemistry in the Steel and Metals Industries*, ed. R. Tomellini, European Communities, Luxembourg, 1999, pp. 47–54.
4 V.-D. Hodoroaba, V. Hoffmann, E. B. M. Steers and K. Wetzig, *J. Anal. At. Spectrom.*, 2000, **15**, 951.
5 V.-D. Hodoroaba, V. Hoffmann, E. B. M. Steers and K. Wetzig, *J. Anal. At. Spectrom.*, 2000, **15**, 1075.
6 V.-D. Hodoroaba, E. B. M. Steers, V. Hoffmann and K. Wetzig, *J. Anal. At. Spectrom.*, 2001, **16**, 43.
7 R. S. Mason, P. D. Miller and I. P. Mortimer, *Phys. Rev. E*, 1997, **55**, 7462.
8 M. Kuraica and N. Konjevic, *Phys. Rev. A*, 1992, **46**, 4429.
9 M. Kuraica, N. Konjevic, M. Platisa and D. Pantelic, *Spectrochim. Acta, Part B*, 1992, **47**, 1173.
10 I. R. Videnovic, N. Konjevic and M. Kuraica, *Spectrochim. Acta, Part B*, 1996, **51**, 1707.
11 P. F. Knewstubb and A. W. Tickner, *J. Chem. Phys.*, 1962, **36**, 674.
12 M. H. Gordon and C. H. Kruger, *Phys. Fluids B*, 1993, **5**, 1014.
13 R. F. G. Meulenbroeks, A. J. van Beek, A. J. G. van Helvoort, M. C. M. van de Sanden and D. C. Schram, *Phys. Rev. E*, 1994, **49**, 4397.
14 F. L. Tabares and D. Tafalla, *J. Vac. Sci. Technol. A*, 1996, **14**, 3087.
15 C. V. Budtz-Jorgensen, P. Kringhoj and J. Bottiger, *Surf. Coat. Technol.*, 1999, **116**, 938.
16 J. T. Gudmundsson, *Plasma Sources Sci. Technol.*, 1999, **8**, 58.
17 A. Manenschijn, G. C. A. M. Janssen, E. van der Drift and S. Radelaar, *J. Appl. Phys.*, 1991, **69**, 1253.
18 S. B. Radovanov, J. K. Olthoff, R. J. Van Brunt and S. Djurovic, *J. Appl. Phys.*, 1995, **78**, 746.
19 B. Müller, Ch. Ottinger and M. Yang, *Z. Phys. A*, 1985, **320**, 61.
20 M. A. A. Clyne, M. C. Heaven, K. D. Bayes and P. B. Monkhouse, *Chem. Phys.*, 1980, **47**, 179.
21 K. R. Ryan and I. G. Graham, *J. Chem. Phys.*, 1973, **59**, 4260.
22 P. Tosi, *Chem. Rev.*, 1992, **92**, 1667.
23 N. Sadeghi and D. W. Setser, *Chem. Phys.*, 1985, **95**, 305.
24 N. G. Adams, D. K. Bohme, D. B. Dunkin and F. C. Fehsenfeld, *J. Chem. Phys.*, 1970, **52**, 1951.
25 A. E. Roche, M. M. Sutton, D. K. Bohme and H. I. Schiff, *J. Chem. Phys.*, 1971, **55**, 5480.
26 V. Aquilanti, A. Galli, A. Giardini-Guidoni and G. G. Volpi, *J. Chem. Phys.*, 1965, **43**, 1969.
27 C. R. Lishawa, J. W. Feldstein, T. N. Stewart and E. E. Muschlitz Jr., *J. Chem. Phys.*, 1985, **83**, 133.
28 A. V. Phelps, *J. Phys. Chem. Ref. Data*, 1992, **21**, 883.
29 B. L. Peko, R. L. Champion and Y. Wang, *J. Chem. Phys.*, 1996, **104**, 6149.
30 B. L. Peko and R. L. Champion, *J. Chem. Phys.*, 1997, **107**, 1156.
31 I. N. Brovikova, E. G. Galiaskarov, A. M. Islyaikin and V. I. Svetsov, *High Temperature*, 1999, **37**, 503.
32 T. G. Beuthe and J.-S. Chang, *Jpn. J. Appl. Phys.*, 1999, **38**, 4576.
33 A. Bogaerts and R. Gijbels, *J. Anal. At. Spectrom.*, 2000, **15**, 441.
34 A. Bogaerts and R. Gijbels, *Spectrochim. Acta, Part B,* submitted for publication.
35 A. Bogaerts and R. Gijbels, *Phys. Rev. A*, 1995, **52**, 3743.
36 A. Bogaerts, M. van Straaten and R. Gijbels, *J. Appl. Phys.*, 1995, **77**, 1868.
37 A. Bogaerts and R. Gijbels, *J. Appl. Phys.*, 1996, **79**, 1279.
38 A. Bogaerts and R. Gijbels, *Anal. Chem.*, 1996, **68**, 2676.
39 A. Bogaerts, R. Gijbels and W. J. Goedheer, *Anal. Chem.*, 1996, **68**, 2296.
40 M. Müller, Ph.D. Thesis, Universität Essen, 1997.
41 N. Matsunami, Y. Yamamura, Y. Itikawa, N. Itoh, Y. Kazumata, S. Miyagawa, K. Morita, R. Shimizu and H. Tawara, *At. Data Nucl. Data Tables*, 1984, **31**, 1–80.
42 A. Bogaerts and R. Gijbels, *J. Anal. At. Spectrom.*, 1996, **11**, 841.